The Phonon Theory of Liquids and Biological Fluids: Developments and Applications

Dima Bolmatov*,†,‡

†Department of Physics and Astronomy, University of Tennessee, Knoxville, TN 37996,
United States

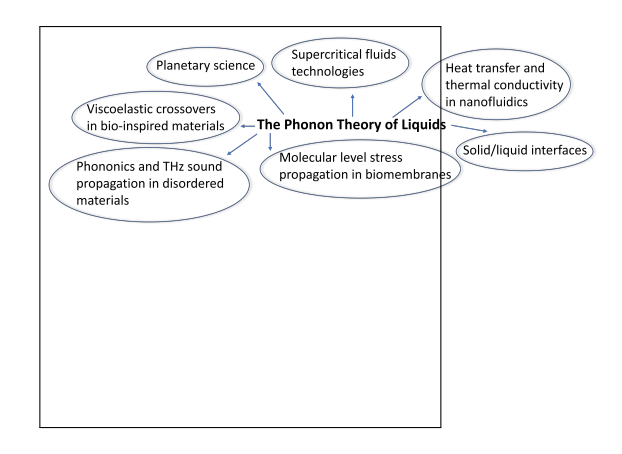
‡Shull Wollan Center, Oak Ridge National Laboratory, Oak Ridge, TN 37831, United
States

E-mail: dbolmato@utk.edu,dbolmatov@ornl.gov

Abstract

Among the three basic states of matter, solid, liquid, and gas, the liquid state has always eluded general theoretical approaches for describing liquid energy and heat capacity. In this Viewpoint, we derive the phonon theory of liquids and biological fluids stemming from Frenkel's microscopic picture of the liquid state. Specifically, the theory predicts the existence of phonon gaps in vibrational spectra of liquids and a thermodynamic boundary in the supercritical state. Direct experimental evidence reaffirming these theoretical predictions was achieved through a combination of techniques using static compression X-ray diffraction and inelastic X-ray scattering on deeply supercritical argon in a diamond anvil cell. Furthermore, these findings have inspired and then led to the discovery of phonon gaps in liquid crystals (mesogens), block copolymers, and biological membranes. Importantly, phonon gaps define viscoelastic crossovers in cellular membranes responsible for lipid self-diffusion, lateral molecular-level stress propagation, and passive transmembrane transport of small molecules and solutes. Finally, molecular interactions mediated by external stimuli result in synaptic activity controlling biological membranes' plasticity resulting in learning and memory. Therefore, we also discuss learning and memory effects - equally important for neuroscience as well as for developments of neuromorphic devices – facilitated in biological membranes by external stimuli.

TOC Graphic



Phonons are quantized vibrations of atoms and molecules in crystalline solids, also known as quantized normal modes. These quantum mechanical quasiparticles are massless and behave like particles in momentum space (i.e., kspace). Importantly, phonons play the central role in the Debye theory of solids, where the solid is treated as N non-interacting harmonic oscillators.² The theory was originally introduced in 1912 and adequately covers low temperature (Debye T^3 -law) and high temperature behavior (Dulong-Petit law) of the specific heat of solids.² The heat capacity of materials, both classical and quantum, is one of the most important thermodynamic properties and the phonon theory has enjoyed a century of success in describing this property in the solid state. Despite this rapid and sustained success of the atomistic description of solids in early 20th century, ²⁻⁴ a similarly powerful, molecular theory of liquids – accounts for the mathematically general expression for liquid energy and heat capacity – remained elusive for the following century.⁵

The historical gap between the theories of heat capacity for liquid and solid states has a few explanations. First, intermolecular interactions in liquids are system specific and strong, while molecular displacements are large. this regard, the formulation of a mathematically rigorous, general theory of liquids has never been considered as practically feasible. Second, this sentiment was predominantly advocated by Landau's school, which was very influential at the time. Specifically, Landau's argument was rooted in the fact that vibrational energies of liquids cannot be calculated in general form due to the lack of a small parameter, implying that it is not physically justified to expand the internal energy of a liquid in terms of squared atomic displacements, as it was done in the phonon theory of solids.² At the same time, Frenkel did not follow the popular trend of the time. Notably, Frenkel's profound physical intuition helped him to keenly elaborate on a microscopic picture of the liguid state. As a result, Frenkel's genuine idea – not mathematically rigorous though – inspired further theoretical activity, eventually leading to the development of a theory for the specific heat capacity of liquids using frameworks based on the solid state approach, bridging the halfcentury historical gap. ^{8,9}

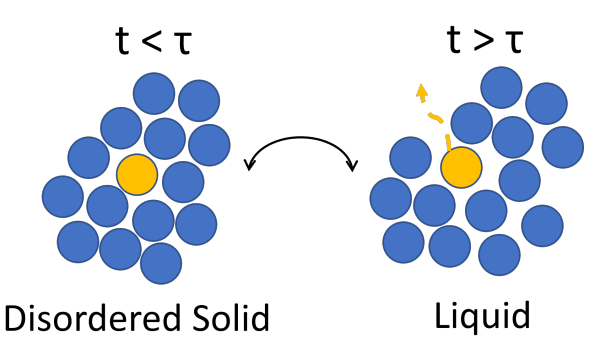


Figure 1: A microscopic picture of a relaxation process in a liquid with a characteristic relaxation time τ proposed by Frenkel.^{5,7} It represents atomic jumps of a reference atom (orange) with respect to its neighboring atoms (blue) as a result of their two consecutive rearrangements. At times shorter than the relaxation time τ , the atomistic neighborhood of the reference atom is practically a disordered solid, implying that both compression and shear elastic waves can pass through. However, at longer times, when a local atomic neighborhood is structurally rearranged and relaxed, it is practically a liquid, where shear elastic waves are not supported anymore.

There are additional reasons for the delay in the development of the phonon theory of liquids. First, the liquid state was historically approached from the gas phase, where specific intermolecular interactions were treated as small perturbations, including but not limited to the virial expansions, cluster expansions, Meyer expansions, Percus-Yevick based approaches, and hard-spheres models, ^{10,11} to name a few. Second, and perhaps a more significant reason for the time lag, was the relatively slow development of cutting-edge experimental techniques to probe molecular interactions in liquids such as energy transfer-resolved and momentum transfer-resolved inelastic X-ray and neutron scattering (IXS/INS). 12-15

Fig. (1) schematically illustrates a microscopic picture of a relaxation process in a liquid

proposed by Frenkel.^{5,7} Specifically, Frenkel introduced a relaxation time τ , which can be defined as the average time between two consecutive, local rearrangements of neighboring atoms (blue) surrounding a reference atom (orange). Such consecutive atomic jumps result in the process of liquid flow from a microscopic point of view. Importantly, this microscopic picture of liquids implies that at short times $(t < \tau)$ the molecular neighborhood of a reference atom, see Fig. (1), is practically a disordered solid, and as such it is able to support both the propagation of compression and shear waves. However, at longer times $(t > \tau)$ the reference atom is able to diffuse away from its atomic neighborhood, due to its local structural rearrangements, losing the ability to be responsive to elastic shear waves. Furthermore, this microscopic picture of the liquid state was taken into account as the molecular basis for the development of the phonon theory of liquids. 5 As a result, the existence of a new thermodynamic boundary in the supercritical state was proposed, ^{16–19} and dubbed the Frenkel line. 16

In general, the vibrational density of states $g(\omega)$ defines the number of phonon states in the reciprocal **k**-space of a angular frequency ω in a given frequency interval between ω and $\omega + d\omega$. The density of states reads as:

$$g(\omega) = \frac{\omega^2}{k_{\rm D}^3} \left[\left(\frac{k^2}{\omega^2} \frac{\partial k}{\partial \omega} \right)_{\rm L} + 2 \left(\frac{k^2}{\omega^2} \frac{\partial k}{\partial \omega} \right)_{\rm T} \right], \quad (1)$$

where L and T stand for longitudinal and transverse phonon modes, respectively. ⁶ In contrast to the Einstein approximation, where the phonon density of states is represented by the Dirac δ -function, ^{3,4} we have $g(\omega) \sim \omega^2$ in the Debye approximation. ² Therefore, the number of phonon states $g(\omega)d\omega$ having angular frequencies between ω and $\omega + d\omega$ is given by:

$$g(\omega) = \frac{V}{2\pi^2} \left[\frac{1}{c_l^3} + \frac{2}{c_t^3} \right] \equiv \frac{9N\omega^2}{\omega_D^3} \left(\omega \le \omega_D \right) \quad (2)$$

$$g(\omega) = 0 \qquad (\omega > \omega_{\rm D}),$$
 (3)

where c_l and c_t are the longitudinal and transverse sounds velocities, and ω_D is the highest frequency supported in a system, namely the

Debye frequency. As a result, the Debye frequency is determined by:

$$\int_0^{\omega_{\rm D}} g(\omega) d\omega \equiv 3N,\tag{4}$$

where N is the number of atoms.² The sound velocity in a system depends on the direction of the sound propagation, which means that, generally, $c_l \neq c_t$. Here, we will use the Debye approximation in which

$$c_l = c_t = c$$
 so that $\omega_k = ck$ (5)

This is important in the phonon theory of liquids as we expect liquids to remain isotropic, ⁵ without any high-symmetry directions as in crystalline solids. ¹

A general expression for liquid energy can be derived on the basis of a standard statistical mechanics procedure by defining a partition function of a liquid. 6,11 The partition function Z for a liquid system of identical harmonic oscillators can be written as:

$$Z = \prod_{j} Z_{j},\tag{6}$$

where oscillators numbered by j, and more explicitly as:

$$\prod_{j} Z_{j} = \sum_{0}^{\infty} e^{\frac{-(n + \frac{1}{2})\hbar\omega_{j}}{k_{\mathrm{B}}T}} = \left[2\sinh\left[\frac{\hbar\omega_{j}}{2k_{\mathrm{B}}T}\right]\right]^{-1},$$
(7)

where ω_j is the angular frequency, T is the temperature, $k_{\rm B}$ is the Boltzmann constant. Once the system's partition function has been calculated, the free energy, $F = -k_{\rm B}T \ln Z$, is given by:

$$F = E_0 + k_{\rm B}T \sum_{j} \ln\left(1 - e^{-\frac{\hbar\omega_j}{k_{\rm B}T}}\right), \quad (8)$$

where E_0 is the zero-point energy. Taking into account the effect of thermal expansion $\left(\frac{\partial \omega}{\partial T} \neq 0\right)$ the internal energy, $^{5,9}E = -T^2 \left[\frac{\partial}{\partial T} \left(\frac{F}{T}\right)\right]_{\rm V,N}$, is given by:

$$E = E_0 + \hbar \sum_j \frac{\omega_j - T \frac{d\omega_j}{dT}}{e^{\frac{\hbar \omega_j}{k_B T}} - 1}$$
 (9)

Furthermore, we use quasi-harmonic Grüneisen approximation,⁹ which results in $\frac{\partial \omega}{\partial T} = -\frac{\alpha \omega}{2}$, where α is the coefficient of thermal expansion.^{5,9} Incorporating the expression for the thermal expansion into Eq. (9) gives:

$$E = E_0 + \left(1 + \frac{\alpha T}{2}\right) \sum_j \frac{\hbar \omega_j}{e^{\frac{\hbar \omega_j}{k_{\rm B}T}} - 1}$$
 (10)

Finally, a general expression for liquid energy in the framework of the phonon theory of liquids – no low-frequency shear phonon contributions: $\omega_j < \omega_{\rm F}$ – with incorporated anharmonic effects reads as: ⁵

$$E = NT \left[1 + \frac{\alpha T}{2} \right] \left[3D \left(\beta \hbar \omega_{\rm D} \right) - \frac{\omega_{\rm F}^3}{\omega_{\rm D}^3} D \left(\beta \hbar \omega_{\rm F} \right) \right], \tag{11}$$

where $D(\sigma) = \frac{3}{\sigma^3} \int_0^{\sigma} \frac{x^3 dx}{e^x - 1}$ is the Debye function, $\omega_{\rm F}$ is the Frenkel frequency, $\beta = (T)^{-1}$ is the reciprocal of temperature T, where $k_{\rm B} = 1$. Importantly, $\omega_{\rm F}$ defines the lower frequency bound for transverse phonon excitations. 5,9 Eq. (11) spans both quantum and classical limits. It is noteworthy that this framework for the phonon theory of liquids has successfully predicted 21 different liquid energies and heat capacities of monatomic noble liquids and molecular liquids such as hydrogen sulphide, methane, and hydrogen-bonded network liquids. 5 Specifically, the theory was able to reproduce a drop in heat capacity $(c_V = \left(\frac{1}{N} \frac{\partial E}{\partial T}\right)_{\rm N}$: $3k_{\rm B} \stackrel{T}{\to} 2k_{\rm B}$) within wide temperature ranges, in a good agreement with experimental data. 5 The Frenkel frequency $\omega_{\rm F}$ is calculated via

$$\omega_{\rm F}(T) = \frac{2\pi}{\tau(T)} = \frac{2\pi G_{\infty}}{\eta(T)},\tag{12}$$

where G_{∞} is the infinite-frequency shear modulus, η is the viscosity, and $\tau \equiv \frac{\eta}{G_{\infty}}$ is the Maxwell relationship for the relaxation time τ originally introduced in 1867.²⁰ Experimentally measured viscosities of liquids are available at the National Institute of Standards and Technology (NIST) database (https://webbook.nist.gov/chemistry/fluid/).

In the early 1800s, Dulong and Petit proposed a thermodynamic law for specific heat capacity c_V of different chemical elements in the solid

phase stating that it is constant $-c_V = 3k_{\rm B}$ – at temperatures far beyond the absolute zero. Here, we can immediately derive this empirically observed result from Eq. (11). First, we recall an important limit of the Debye function: $D(\sigma) = 1$, when $\sigma \longrightarrow 0$. Therefore, $D\left(\frac{\hbar\omega_{\rm D}}{k_{\rm B}T}\right) \longrightarrow 1$ at elevated temperatures in the $T \longrightarrow \infty$ limit. As a result, liquid energy and specific heat capacity in the classical limit reads as:

$$E = 3Nk_{\rm B}T \left(1 + \frac{\alpha T}{2}\right)$$

$$c_V = \frac{C_V}{N} = 3k_{\rm B}(1 + \alpha T),$$
(13)

where $\omega_{\rm F}=0$ in the solid phase. Finally, the Dulong-Petit law derived in the harmonic approximation ($\alpha=0$) from Eq. (11) reads as:

$$c_V = k_{\rm B} \frac{\partial}{\partial T} \cdot T(1+0)(3 \cdot 1 - 0 \cdot 1) = 3k_{\rm B}$$
 (14)

Mind the phonon gaps. Importantly, the phonon theory of liquids can be derived on a more general basis by introducing a Hamiltonian: 21,22 $H = H_0 + H_{int}$. H_0 describes the dynamics of the phonon field in a harmonic approximation:

$$H_0 = \frac{1}{2} \sum_{\omega_k < \omega_D} \left[\prod_k^{\gamma} \prod_{-k}^{\gamma} + \mu \omega_k^2 Q_k^{\gamma} Q_{-k}^{\gamma} \right]$$
 (15)

and H_{int} represents higher order phonon interactions:

$$H_{\text{int}} = \sum_{\omega_k < \omega_D} \left[-\frac{g}{2} |Q_k^{\gamma}|^4 + \frac{\lambda}{6} |Q_k^{\gamma}|^6 \right]$$
 (16)

Here, k is the multi-index $\{k_1, k_2, k_3\}$ for the wavevector values corresponding to three spatial directions, μ is a parameter that takes a value 1 or 0, and $\gamma = (l, t, t)$ is another set of indices with l and t standing for the longitudinal and transverse phonon modes, respectively. The parameters $g, \lambda \in \mathbb{R}^+$ are real nonnegative coupling parameters. Π_k^{γ} and Q_k^{γ} are collective canonical coordinates, where $|Q_k^{\gamma}| = (Q_k^{\gamma} Q_{-k}^{\gamma})^{1/2}$. When $\omega_k < \omega_F$, the potential terms in the Hamiltonian [second term in Eq. (15) combined with both terms in Eq. (16)]

have minima which break the rotational symmetry of the phonon excitations from SO(3) to SO(2). Phonon excitations around the ground state \bar{Q}_k^{γ} can be written as: $Q_q^{\gamma} = \bar{Q}_k^{\gamma} + \varphi_k^{\gamma}$, where φ_k^l and $\varphi_k^{t,t}$ are longitudinal and transverse phonon scalar fields. For a chosen vacuum state, i. e., the lowest energy state in a field which breaks the rotational symmetry when $\omega_k < \omega_F$, we have $\bar{Q}_k^{\gamma} = \delta_k^1 |\bar{Q}_k^{\gamma}|$ and the effective Hamiltonian for the excitations around this state reads

$$H[\varphi_{k}] = \frac{1}{2} \sum_{0 \leq \omega_{k} \leq \omega_{D}} [\Pi_{k}^{l,t,t} \Pi_{-k}^{l,t,t}] + \frac{1}{2} \sum_{0 \leq \omega_{k} \leq \omega_{D}} [\omega_{k}^{2} \varphi_{k}^{l} \varphi_{-k}^{l}] + \sum_{\omega_{F} \leq \omega_{k} \leq \omega_{D}} [\omega_{k}^{2} \varphi_{k}^{t,t} \varphi_{-k}^{t,t}]$$

$$(17)$$

The effective Hamiltonian is the operator corresponding to the total energy E of a system in the liquid state, $H\varphi = E\varphi$, including both kinetic energy and potential energy in Eq. (11). It has a subtle spectral feature regarding low-frequency transverse phonon excitations [see last term in Eq. (17)]. Specifically, low-frequency transverse phonon excitations are heavily overdamped due to non-linear phonon interactions. The absence of these excitations was dubbed phonon gaps ($0 \le \omega_k^{t,t} <$ $\omega_{\rm F}$). ^{21,22} Furthermore, the existence of phonon gaps – energy transfer E-gap and momentum transfer Q-gap – in spectra of liquid argon was observed via inelastic X-ray scattering (IXS) in a diamond anvil cell.²³

Thermally triggered, overdamped frequency shear elastic waves (transverse phonon gaps) result in a disappearance of the long-range order pair correlations. 23 Furthermore, the temperature increase leads to the progressive disappearance of both medium-range order pair correlations and high-frequency transverse phonon excitations ($\omega_{\rm F} \leq \omega_k^{t,t} \xrightarrow{T} \omega_{\rm D}$, therefore, c_V : $3k_B \xrightarrow{T} 2k_B$). A complete disappearance of both high-frequency transverse phonon excitations in the harmonic approximation ($\alpha = 0$, $\omega_{\rm F} = \omega_{\rm D}$, $c_{\rm V} = 2k_{\rm B}$, see Eq. (11)), and medium-range order pair correlations is the manifestation of the new ther-

New thermodynamic boundary on the P-T phase diagram

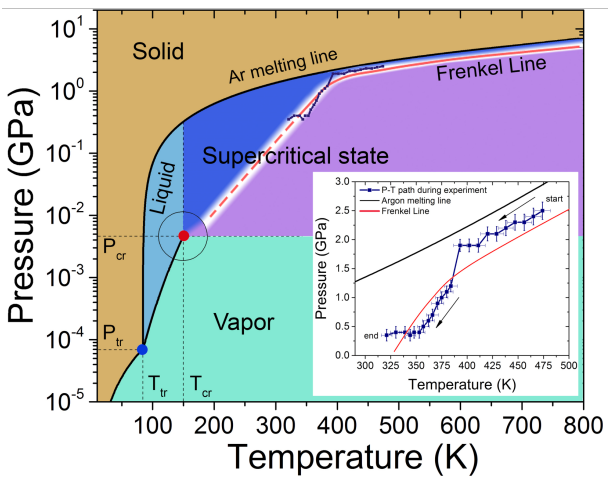


Figure 2: Argon pressure-temperature, P-T, phase diagram with a newly discovered thermodynamic boundary, adapted from Bolmatov $et\ al.^{24}$ Compelling experimental evidence of the boundary was provided through static compression X-ray diffraction 24 and inelastic X-ray scattering on deeply supercritical argon in a diamond anvil cell. 25 The inset shows the experimental P-T path over X-ray diffraction measurements. 24

modynamic boundary (see Fig. 2) on the pressure-temperature phase diagram, dubbed the Frenkel line. 16 Direct, compelling experimental evidence for the new thermodynamic boundary demarcating liquid-like and gas-like subdomains of the supercritical state - a single state, ^{24,25} rather than the previously erroneously assumed two states of matter 16was achieved through static compression X-ray diffraction and IXS in a diamond anvil cell on deeply supercritical argon. ^{24,25} As a result, this experimental evidence has stimulated much interest in studying a myriad of thermodynamic, structural, and dynamic properties of supercritical state in the vicinity of the Frenkel line and beyond. $^{26-48}$

The phonon theory of liquids has also been widely utilized as a theoretical framework in applied and fundamental research such as nanofluidics, supercritical fluids technologies, confined liquids, heat transfer and thermal conductivity, solid/liquid interfaces, and planetary science, ^{49–85} to name a few. For instance, it was demonstrated that in gas giants such as Jupiter and Saturn, supercritical hydrogen has a crossover in all its major thermodynamic properties at approximately 10 GPa and 3000 K. As a result, determination of the Frenkel line in supercritical H₂ enabled a demarcation of the boundary between interior and atmosphere in gas giants. 86 Moreover, a precise location of the Frenkel line's thermodynamic boundary in supercritical CO₂ revived the long-standing question whether Venus may have had carbon dioxide oceans, which presumably influenced the formation of the present terrestrial landscape of the planet. 87 The theory was also used in studying exotic properties of liquid helium at elevated pressures and supercritical temperatures. Unexpectedly, it was discovered that liquid ⁴He in the very wide pressure range (5 MPa-500 MPa) is both solid-like and quantum.⁸⁸

En route from simple liquids to biological fluids. The existence of phonon gaps $(0 \le \omega_k^{t,t} < \omega_{gap})$, where ω_{gap} is the lower frequency bound for transverse phonon excitations) in vibrational spectra of liquids inspired a further search for such spectral gaps in complex, soft (non-crystalline) and biological materials. In-

deed, the field theoretic approach - the effective Hamiltonian, Eq. (17) – was derived on a general basis, implying that any disordered materials may have spectral, transverse phonon gaps as a result of the overdamped nature of shear elastic waves beyond their shortrange propagation. However, there is a limited number of experimental techniques capable of probing collective motions at the molecular level. IXS/INS are unique examples of non-invasive, ^{12–14} energy transfer-, and momentum transfer-resolved spectroscopy techniques, enabling measurements of collective, shortlived (picoseond), and short-range (nanometer) phonon gaps and phonon excitations of disordered materials. These measured excitations and their vibrational patterns can be described by the theoretical framework, see Eq. (17). Furthermore, phonon gaps in soft (disordered, non-crystalline) materials have been experimentally observed, for the first time, using IXS in liquid crystals (mesogens), ^{89,90} block copolymers, 53 and most importantly in biological membranes. 91,92

Biological membranes are two-dimensional (2D) fundamental building blocks of cells, defining the boundaries between their extracellular and intracellular biological fluids. fact, biomembranes are semi-permeable 2D fluids, and are also found in eukaryotic cellular organelles such as the nucleus, autophagosomes, chloroplasts, and mitochondria, containing the molecular machinery to facilitate their different functions. 93 Dipalmitoylphosphatidylcholine (DPPC) bilayer is a phospholipid the major phospholipid constituent of the pulmonary (lung) surfactant – consisting of two hydrophobic tails (palmitic acids) attached to hydrophilic headgroup (phosphatidylcholine).⁹¹ DPPC lipids can be used to create phospholipid membranes that contain two leaflets. Figure 3 (a) shows the IXS scattering geometry of the DPPC bilayer. In IXS experiments, 94 an incident X-ray beam of energy E_i and momentum $\mathbf{k}_i - \hbar = 1$ – scatters away with energy E_f and momentum \mathbf{k}_f mainly due to interactions with electrons, see Figure 3(a). Importantly, phonon excitations originate from thermallytriggered density-density fluctuations. As a re-

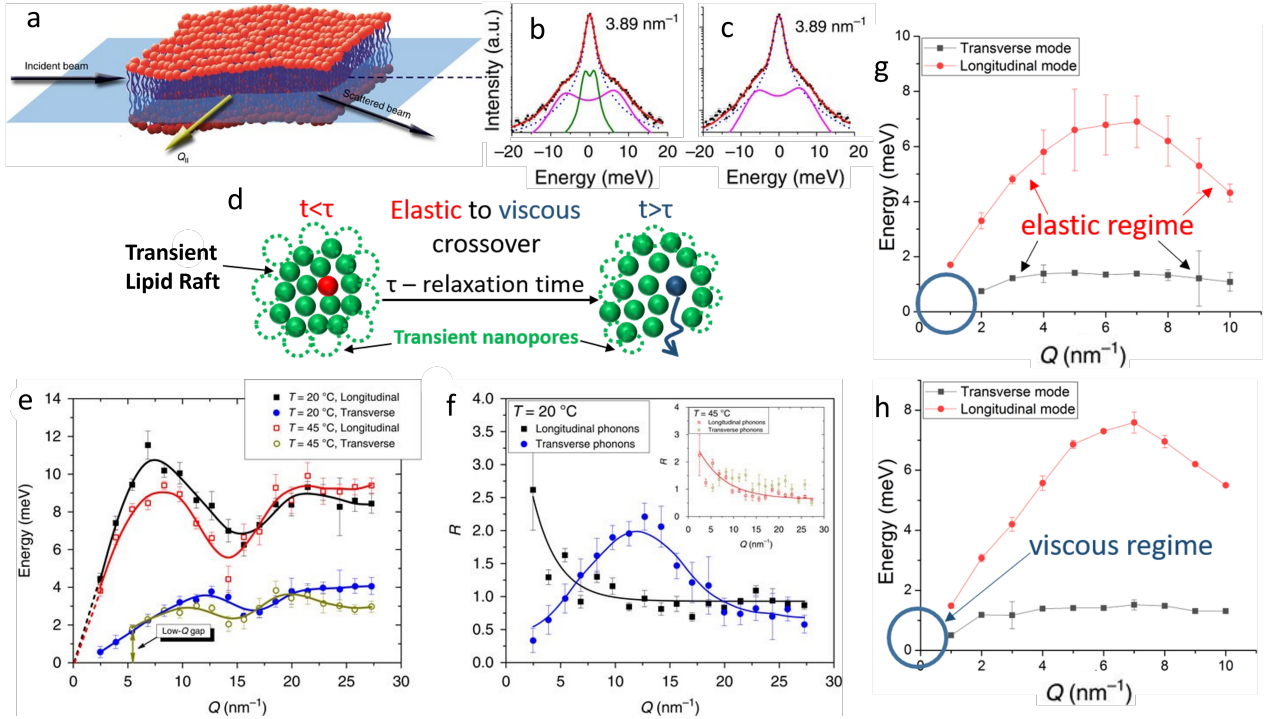


Figure 3: Phonon excitations, phonon gaps, and viscoelastic crossovers in biological membranes. (a) Schematic of the IXS scattering geometry of phospholipid bilayers. The scattering plane is orthogonal to the figure plane. IXS selected spectra at $Q=3.89~\mathrm{nm}^{-1}$ of a DPPC membrane, measured within -20 meV - 20 meV energy range, at 20 °C in the gel phase (b) and at 45 °C in the fluid phase (c), respectively. (d) Schematic illustration of a elastic-to-viscous crossover experienced by a transient lipid raft that is surrounded by transient nanopores/membrane voids. As a result, this relaxation process of transient lipid rafts enables the lateral molecular level mechanical stress propagation in biomembranes. (e) Longitudinal and transverse phonon modes of the DPPC membrane providing first compelling experimental evidence for a thermally triggered Q-gap (phonon gap) in biological materials. (f) Damping ratios $R = \frac{\omega(Q)}{\Gamma(Q)}$ of longitudinal and transverse phonon modes are presented as a function of Q in the gel phase, and in the fluid phase (see inset). (g,h) IXS vibrational spectra at a physiologically relevant temperature of 37 °C of fluid phase DMPC-Cholesterol-Melatonin membranes. The presence of 27 mol% melatonin leads to the acoustic phonon gap closing.

sult, the scattered beam carries information on phonons corresponding to the scanned energy transfer $E = E_f - E_i$ and momentum transfer $\mathbf{Q} = \mathbf{k}_f - \mathbf{k}_i$. Furthermore, IXS phonon spectra and their spectral lineshapes, see Figure 3(b,c), can be fitted utilizing the Damped Harmonic Oscillator (DHO) model given by:

DHO =
$$\sum_{j=0}^{N} \frac{A_j(Q)\Gamma_j(Q)E_j^2(Q)E^2}{(E^2 - E_j^2(Q))^2 + (\Gamma_j(Q)E)^2},$$
(18)

where E_j is the average excitation energy, $A_j(Q)$ is the amplitude of a single inelastic $(E_j \neq 0)$ phonon excitation, and $\Gamma_j(Q)$ is

the half-width at half-maximum of a vibrational peak. 94 Each selected IXS spectrum has a specific number of vibrational peaks within a scanned energy range. In Figure 3 b and c are IXS spectra at $Q=3.89~\rm nm^{-1}$ of the DPPC bilayer in the gel phase at 20 °C and in the fluid phase at 45 °C, respectively. The experimental data (black squares) with error bars are displayed along with the best least squares fits (red solid curves) utilizing the DHO model with two phonon excitations. Low- and high-energy DHOs are depicted as green and magenta solid lines, respectively. Importantly, the temperature increase from 20 °C to 45 °C tran-

sitioning from the gel to fluid phase leads to the emergence of low-(E, Q) phonon gap in the vibrational spectrum of the DPPC phospholipid membrane, see the green line is absent in Figure 3 (c).⁹¹ This was the first experimental evidence for the existence of phonon gaps in biological fluids reaffirming the predictions from the field theoretical approach, see Eq. (17). The existence of phonon gaps in DPPC phospholipid bilayers was then successfully validated through Brillouin neutron scattering measurements. 95 As a result, a molecular level mechanism was proposed for transient lipid rafts (domains) surrounded by transient nanopores (voids) responsible for the in-plane self-diffusion of lipids, molecular-level mechanical stress propagation, and passive transmembrane transport of small molecules (H₂O, O₂, CO_2) and solutes, ⁹⁶ see Figure 3(d). It is worth noting that boundaries of lipid rafts (domains) have fractal dimensions. 97

Furthermore, each set of (E,Q) points corresponds to a single phonon mode, either longitudinal or transverse branch, see Figure 3 (e). Therefore, a precise determination of low-(E,Q) phonon gaps from the vibrational spectra enables the determination of the size and lifetime of lipid rafts (domains), also known as lateral membrane heterogeneities. ally, closing of the phonon gap can be achieved upon cooling a biomembrane as a result of its viscosity drop, see Eq. (12).Intriguingly, inclusion of exogenous molecules such as 27 mol% melatonin – a hormone also indigenously produced by the brain's pineal gland 98 that strongly interacts with phospholipid headgroups of cholesterol-enriched dimvristovlphosphatidylcholine (DMPC) bilayers results in the (E, Q) phonon gap closing as well, ⁹² see This finding highlights the Figure 3 (h). protective properties of melatonin, where it acts as a surfactant to preserve the structural integrity of biomembranes. 99 A stabilization property of melatonin was also observed in both nanometer- and micrometer-sized liposomes utilizing small angle neutron scattering (SANS) combined with confocal fluorescence microscopy and differential scanning calorimetry (DSC). 100

Importantly, vibrational landscapes of biological membranes can also be studied through calculation of the longitudinal $C_L(Q, E)$ and transverse $C_T(Q, E)$ current correlation spectra employing molecular dynamics simulations. Specifically, phonon modes can be calculated via the projection of lipid correlation functions in directions along and perpendicular to the wavevector \vec{Q} parallel to the surface of the membrane. Section 5.101 Furthermore, current correlation spectra $C_{\gamma}(\vec{Q}, E)$ can be represented as:

$$C_{\gamma}(\vec{Q}, E) \equiv \int_{-\infty}^{+\infty} dt \ e^{iEt} \langle \vec{J}_{\gamma}^{*}(\vec{Q}, t) \cdot \vec{J}_{\gamma}(\vec{Q}, t) \rangle,$$
(19)

where $\gamma = (L \text{ - longitudinal}; T \text{ - transverse}),$ and the corresponding time-dependent current-current correlation functions given by:

$$\vec{J}_L(\vec{Q},t) = \frac{1}{\sqrt{N}} \sum_{m} \hat{\vec{Q}} (\hat{\vec{Q}} \cdot \vec{v}_m(t)) e^{-i\vec{Q} \cdot \vec{r}_m(t)} (20)$$

$$\vec{J}_T(\vec{Q},t) = \frac{1}{\sqrt{N}} \sum_{m} \hat{\vec{Q}} \times \vec{v}_m(t) e^{-i\vec{Q} \cdot \vec{r}_m(t)} (21)$$

where $\hat{\vec{Q}}$ is the unit vector along \vec{Q} , N is the total number of molecules, and $\vec{r}_m(t)$ and $\vec{v}_m(t)$ are coordinates and velocities of molecule m, respectively. Thereafter, both longitudinal and transverse phonon modes of biomembranes including their phonon gaps can readily be obtained by fitting $C_L(Q, E)$ and $C_T(Q, E)$ using the DHO model. ⁹⁶

Furthermore, the self-diffusion coefficient D_l can be written as:

$$D_l = \frac{k_{\rm B}T}{f} e^{-\frac{A_r}{A_v}},\tag{22}$$

where k_B is the Boltzmann constant, T is the temperature, f is the translational drag friction parameter, $^{105}A_r = \frac{\pi d^2}{4}$ is the area of a transient lipid raft (domain), $d = \frac{2\pi}{Q_{gap}}$ is the diameter of the void ring, Q_{gap} is the reciprocal space phonon gap, see Figure 3(e,f,g), $A_v = \pi dL$ is the area of the void ring around the lipid raft. Finally, the temperature dependent self-diffusion coefficient can be represented as: 92,96

$$D_l(T) = \frac{k_{\rm B}T}{f} e^{-\frac{1}{2}\frac{\pi\beta(T)}{Q_{gap}(T)R_l}},$$
 (23)

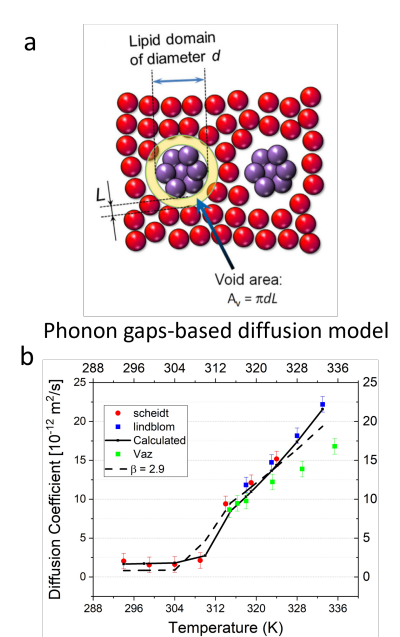


Figure 4: Lateral self-diffusion coefficient $D_L(T)$ of DPPC phospholipid bilayers calculated from Eq. (23) and compared with the experimentally obtained values $^{102-104}$ across three major lipid phases: gel, ripple, and fluid. Black dashed and dotted curves correspond to diffusion coefficients calculated using fixed values of $\beta = 2.86$ and $\beta = 3.23$, respectively. 96

where β is the dimensionless displacement parameter of a lipid within the void ring, R_l is the van der Waals radius of a lipid, and L is the width of the void ring $\frac{R_l}{\beta}$, see Figure 4(a). Finally, Figure 4(b) shows a good agreement between the lateral self-diffusion coefficients calculated from Eq. (23), using temperature-dependent phonon gaps parameters, 96 and experimentally obtained values $^{102-104}$ across all major lipid phases, i.e., gel, ripple, and fluid. 96

Discussion. The Frenkel's microscopic picture of simple liquids⁷ was key for the development of the phonon theory of liquids⁵ and disordered (non-crystalline) materials such as biological fluids at fundamental picosecond time and nanometer length scales. ²¹ However, shear frequency bands at much lower than sub-THz frequencies were experimentally measured in polymer-based melts ^{106–108} and analytically explained in the case of complex confined liquids (0.01 - 0.1 Hz), ¹⁰⁹ potentially relevant for technological advancements capable of heat/energy management and sound manipulation. ¹¹⁰ More-

over, a recently developed analytical model of the vibrational density of states of liquids $(g(\omega) \sim \omega)$ provides new physical insights into universality and low energy behavior of liquids beyond the Debye approximation $(g(\omega) \sim \omega^2)$. 111

On a biologically inspired note, cells have evolved a variety of active and passive mechanisms to regulate the molecular machinery of lipid membranes.⁹³ Among them, the force from lipids (FFLs) is thought to play a crucial role in enabling the cells' different modes of mechanical sensing, including molecular vibrations, sound waves, and changes in cellular volume and shape, 112,113 to name a few. Regarding the molecular pillars of synaptic activity, the membrane-associated molecular mechanisms based on the FFL have historically been underappreciated, but clearly may play a significant role. For example, free fatty acids such as arachidonic acid, released by phospholipase activity on membrane phospholipids, have long been considered beneficial for learning and memory, and are known mediators of neurotransmission and synaptic plasticity. 114 Additionally, membrane-associated processes may also be interconnected with sensing and signal transduction. Specifically, synaptic plasticity describes biological processes that enable learning and memory due to the physicochemical and electromechanical activities between synapses. 115 The resultant patterns from these brain activities can then lead to changes in the connections between individual neurons, a process taking place at the cellular-membrane level, implying that biological membranes with integral ion channels play a key role. 115 By controlling the activity of the nanoscopic poreforming ion channels embedded in membranes, one can manipulate the membrane's resting potential, and other membrane associated signaling, simply by controlling the flow of ions across the cellular membrane. 116,117 In doing so, molecular interactions mediated by external stimuli, e.g., periodic AC voltage waveforms, ¹¹⁸ result in synaptic activity controlling biological membranes' plasticity including their memory resistance (memristance) and memory capacitance (memcapacitance). 117,118 Therefore,

understanding the molecular scale mechanisms underlying synaptic plasticity of membranes is of fundamental importance in gaining insights into the molecular basis of learning and memory. ¹¹⁹

In conclusion, synaptic plasticity of lipid membranes involves intermolecular forces between lipids and ion channels. However, the understanding of these forces at the molecular level is precluded due to a limited number of non-invasive experimental techniques able to access them. 120 Moreover, relatively little is known about how voltage-gated ion channels sense ultrafast (picoseconds/nanoseconds) molecular level FFLs. It is partially due to the fact that most of studies have predominantly focused on the membrane's structural proper-Therefore, the multiscale dynamic processes governed by ultrafast FFLs is terra incoqnita. 94 Consequently, it is still unclear how multiscale FFLs influence the membrane's relaxation processes as a result of cascade-like dynamics, potentially existing as precursor events relevant for energy and memory storage in the form of vibrational patterns such as optical phonons (standing waves). 92,94,121-124 Finally, with the recent development of cutting-edge, non-invasive techniques, enabling the access of vibrational patterns originating from the multiscale FFLs, present great potential for making connections between fundamental, electromechanically mediated molecular mechanisms and biologically-relevant functions.

Acknowledgement DB is supported through the National Science Foundation, Division of Molecular and Cellular Biosciences, under grant no. 2219289. Portions of the computational aspect of this research was supported by the Center for Nanophase Materials Sciences (CNMS), which is a US Department of Energy, Office of Science User Facility at Oak Ridge National Laboratory. DB is also indebted to Maxim O. Lavrentovich and Haden L. Scott for critical reading of the manuscript, and Takeshi Egami, C. Patrick Collier, John Katsaras, and Russel J. Reiter for inspiring discussions.

References

- (1) Ashcroft, N. W.; Mermin, N. D. *Solid State Physics*; Saunders College Publishing, 1976.
- (2) Debye, P. On the Theory of Specific Heats. *Ann. Phys.* **1912**, *39*, 789–839.
- (3) Einstein, A. Planck's Theory of Radiation and The Theory of Specific Heat. *Ann. Phys.* **1907**, *22*, 180–190.
- (4) Rogers, D. Einstein's Other Theory: The Planck-Bose-Einstein Theory of Heat Capacity; Princeton University Press, 2005.
- (5) Bolmatov, D.; Brazhkin, V.; Trachenko, K. The phonon theory of liquid thermodynamics. Sci. Rep. 2012, 2, 1–6.
- (6) Landau, L. D.; Lifshitz, E. M. Statistical *Physics*; Nauka, Moscow, 1964.
- (7) Frenkel, J. Kinetic Theory of Liquids; ed. R. H. Fowler, P. Kapitza, N. F. Mott, Oxford University Press, 1947.
- (8) Trachenko, K. Heat capacity of liquids: An approach from the solid phase. *Phys. Rev. B* **2008**, *78*, 104201.
- (9) Bolmatov, D.; Trachenko, K. Liquid heat capacity in the approach from the solid state: Anharmonic theory. *Phys. Rev. B* **2011**, *84*, 054106.
- (10) Percus, J. K.; Yevick, G. J. Analysis of Classical Statistical Mechanics by Means of Collective Coordinates. *Phys. Rev.* **1958**, *110*, 1.
- (11) Feynman, R. P. Statistical Mechanics: A Set of Lectures; CRC Press, 2018.
- (12) Shirane, G.; Shapiro, S. M.; Tranquada, J. M. Neutron Scattering with a Triple-Axis Spectrometer: Basic Techniques; Cambridge University Press, 2002.

- (13) Hippert, F.; Geissler, E.; Hodeau, J. L.; Lelièvre-Berna, E.; Regnard, J.-R. *Neutron and X-ray Spectroscopy*; Springer Science & Business Media, 2006.
- (14) Cunsolo, A. The Terahertz Dynamics of Simplest Fluids Probed by Inelastic X-ray Scattering. *Int. Rev. Phys. Chem.* **2017**, *36*, 433–539.
- (15) Chen, Z.; Andrejevic, N.; Drucker, N. C.; Nguyen, T.; Xian, R. P.; Smidt, T.; Wang, Y.; Ernstorfer, R.; Tennant, D. A.; Chan, M. et al. Machine Learning on Neutron and X-ray Scattering and Spectroscopies. *Chem. Phys. Rev.* **2021**, *2*, 031301.
- (16) Brazhkin, V.; Fomin, Y. D.; Lyapin, A.; Ryzhov, V.; Trachenko, K. Two Liquid States of Matter: A Dynamic Line on a Phase Diagram. *Phys. Rev. E* 2012, 85, 031203.
- (17) Bolmatov, D.; Brazhkin, V.; Fomin, Y. D.; Ryzhov, V.; Trachenko, K. Evidence for Structural Crossover in The Supercritical State. J. Chem. Phys. **2013**, 139, 234501.
- (18) Bolmatov, D.; Brazhkin, V.; Trachenko, K. Thermodynamic Behaviour of Supercritical Matter. *Nat. Commun.* **2013**, 4, 1–7.
- (19) Brazhkin, V.; Fomin, Y. D.; Lyapin, A.; Ryzhov, V.; Tsiok, E.; Trachenko, K. "Liquid-Gas" Transition in The Supercritical Region: Fundamental Changes in The Particle Dynamics. *Phys. Rev. Lett.* 2013, 111, 145901.
- (20) Maxwell, J. C. IV. On the Dynamical Theory of Gases. *Phil. Trans. Royal Soc. London* **1867**, 49–88.
- (21) Bolmatov, D.; Zav'yalov, D.; Zhernenkov, M.; Musaev, E. T.; Cai, Y. Q. Unified Phonon-Based Approach to The Thermodynamics of Solid, Liquid and Gas States. *Ann. Phys.* **2015**, *363*, 221–242.

- (22) Bolmatov, D.; Musaev, E. T.; Trachenko, K. Symmetry Breaking Gives Rise to Energy Spectra of Three States of Matter. Sci. Rep. 2013, 3, 1–4.
- (23) Bolmatov, D.; Zhernenkov, M.; Zav'yalov, D.; Stoupin, S.; Cunsolo, A.; Cai, Y. Q. Thermally Triggered Phononic Gaps in Liquids at THz Scale. Sci. Rep. 2016, 6, 1–7.
- (24) Bolmatov, D.; Zhernenkov, M.; Zav'yalov, D.; Tkachev, S. N.; Cunsolo, A.; Cai, Y. Q. The Frenkel Line: a direct experimental evidence for the new thermodynamic boundary. *Sci. Rep.* **2015**, *5*, 1–10.
- (25) Bolmatov, D.; Zhernenkov, M.; Zav'yalov, D.; Stoupin, S.; Cai, Y. Q.; Cunsolo, A. Revealing the Mechanism of the Viscous-to-Elastic Crossover in Liquids. J. Phys. Chem. Lett. **2015**, 6, 3048–3053.
- (26) Smith, D.; Hakeem, M.; Parisiades, P.; Maynard-Casely, H.; Foster, D.; Eden, D.; Bull, D.; Marshall, A.; Adawi, A.; Howie, R. et al. Crossover Between Liquidlike and Gaslike Gehavior in CH4 at 400 K. *Phys. Rev. E* **2017**, *96*, 052113.
- (27) Prescher, C.; Fomin, Y. D.; Prakapenka, V.; Stefanski, J.; Trachenko, K.; Brazhkin, V. Experimental Evidence of the Frenkel Line in Supercritical Neon. *Phys. Rev. B* **2017**, *95*, 134114.
- (28) Pazmiño Betancourt, B. A.; Starr, F. W.; Douglas, J. F. String-Like Collective Motion in the α- and β-Relaxation of a Coarse-Grained Polymer Melt. J. Chem. Phys. 2018, 148, 104508.
- (29) Banuti, D.; Raju, M.; Ihme, M. Between Supercritical Liquids and Gases—Reconciling Dynamic and Thermodynamic State Transitions. *J. Supercrit. Fluids* **2020**, *165*, 104895.

- (30) Ruppeiner, G.; Dyjack, N.; McAloon, A.; Stoops, J. Solid-Like Features in Dense Vapors Near the Fluid Critical Point. *J. Chem. Phys.* **2017**, *146*, 224501.
- (31) Pipich, V.; Schwahn, D. Densification of Supercritical Carbon Dioxide Accompanied by Droplet Formation when Passing the Widom Line. *Phys. Rev. Lett.* **2018**, 120, 145701.
- (32) Xie, J.; Liu, D.; Yan, H.; Xie, G.; Boetcher, S. K. A Review of Heat Transfer Deterioration of Supercritical Carbon Dioxide Flowing in Vertical Tubes: Heat Transfer Behaviors, Identification Methods, Critical Heat Fluxes, and Heat Transfer Correlations. Int. J. Heat Mass Transf. 2020, 149, 119233.
- (33) Yoon, T. J.; Lee, Y.-W. Current Theoretical Opinions and Perspectives on the Fundamental Description of Supercritical Fluids. J. Supercrit. Fluids 2018, 134, 21–27.
- (34) Bellissima, S.; Neumann, M.; Guarini, E.; Bafile, U.; Barocchi, F. Density of States and Dynamical Crossover in a Dense Fluid Revealed by Exponential Mode Analysis of the Velocity Autocorrelation Function. *Phys. Rev. E* **2017**, *95*, 012108.
- (35) Mareev, E.; Aleshkevich, V.; Potemkin, F.; Bagratashvili, V.; Minaev, N.; Gordienko, V. Anomalous Behavior of Nonlinear Refractive Indexes of CO2 and Xe in Supercritical States. Opt. Express 2018, 26, 13229–13238.
- (36) Proctor, J.; Pruteanu, C.; Morrison, I.; Crowe, I.; Loveday, J. Transition from Gas-like to Liquid-like Behavior in Supercritical N2. J. Phys. Chem. Lett. **2019**, 10, 6584–6589.
- (37) Ha, M. Y.; Yoon, T. J.; Tlusty, T.; Jho, Y.; Lee, W. B. Universality, Scaling, and Collapse in Supercritical Fluids. *J. Phys. Chem. Lett.* **2019**, *11*, 451–455.

- (38) Mausbach, P.; Köster, A.; Vrabec, J. Liquid State Isomorphism, Rosenfeld-Tarazona Temperature Scaling, and Riemannian Thermodynamic Geometry. *Phys. Rev. E* **2018**, *97*, 052149.
- (39) Raman, A. S.; Li, H.; Chiew, Y. Widom Line, Dynamical Crossover, and Percolation Transition of Supercritical Oxygen via Molecular Dynamics Simulations. *J. Chem. Phys.* **2018**, *148*, 014502.
- (40) Ding, J.; Sun, P.; Huang, S.; Luo, X. Single- and Dual-Mode Rayleigh—Taylor Instability at Microscopic Scale. *Phys. Fluids* **2021**, *33*, 042102.
- (41) Takemoto, A.; Kinugawa, K. Quantumness and State Boundaries Hidden in Supercritical Helium-4: A Path Integral Centroid Molecular Dynamics Study. *J. Chem. Phys.* **2018**, *149*, 204504.
- (42) Pipich, V.; Schwahn, D. Polymorphic Phase Transition in Liquid and Supercritical Carbon Dioxide. *Sci. Rep.* **2020**, *10*, 1–9.
- (43) Chatwell, R. S.; Guevara-Carrion, G.; Gaponenko, Y.; Shevtsova, V.; Vrabec, J. Diffusion of the Carbon Dioxide–Ethanol Mixture in the Extended Critical Region. *Phys. Chem. Chem. Phys.* **2021**, 23, 3106–3115.
- (44) Skarmoutsos, I.; Henao, A.; Guardia, E.; Samios, J. On the Different Faces of the Supercritical Phase of Water at a Near-Critical Temperature: Pressure-Induced Structural Transitions Ranging from a Gaslike Fluid to a Plastic Crystal Polymorph. J. Phys. Chem. B 2021, 125, 10260–10272.
- (45) Pruteanu, C. G.; Kirsz, M.; Ackland, G. J. Frenkel Line in Nitrogen Terminates at the Triple Point. *J. Phys. Chem. Lett.* **2021**, *12*, 11609–11615.
- (46) Jaramillo-Gutiérrez, J.; López-Picón, J.; Torres-Arenas, J. Subcritical and Supercritical Thermodynamic Geometry of

- Mie Fluids. J. Mol. Liq. **2022**, 347, 118395.
- (47) Bell, I. H.; Delage-Santacreu, S.; Hoang, H.; Galliero, G. Dynamic Crossover in Fluids: From Hard Spheres to Molecules. *J. Phys. Chem. Lett.* **2021**, 12, 6411–6417.
- (48) Xu, J.; Wang, Y.; Ma, X. Phase Distribution Including a Bubblelike Region in Supercritical Fluid. *Phys. Rev. E* **2021**, 104, 014142.
- (49) Iacobazzi, F.; Milanese, M.; Colangelo, G.; Lomascolo, M.; de Risi, A. An Explanation of The Al2O3 Nanofluid Thermal Conductivity Based on The Phonon Theory of Liquid. *Energy* **2016**, 116, 786–794.
- (50) Heo, Y.; Antoaneta Bratescu, M.; Aburaya, D.; Saito, N. A Phonon Thermodynamics Approach of Gold Nanofluids Synthesized in Solution Plasma. Appl. Phys. Lett. 2014, 104, 111902.
- (51) Song, D.; Jing, D.; Ma, W.; Zhang, X. Effect of Particle Aggregation on Thermal Conductivity of Nanofluids: Enhancement of Phonon MFP. J. Appl. Phys. 2019, 125, 015103.
- (52) Song, D.; Jing, D.; Ma, W.; Zhang, X. High Thermal Conductivity of Nanoparticles not Necessarily Contributing More to Nanofluids. Appl. Phys. Lett. 2018, 113, 223104.
- (53) Bolmatov, D.; Zhang, Q.; Soloviov, D.; Li, Y. M.; Werner, J. G.; Suvorov, A.; Cai, Y. Q.; Wiesner, U.; Zhernenkov, M.; Katsaras, J. Nanoscale Q-Resolved Phonon Dynamics in Block Copolymers. ACS Appl. Nano Mater. 2018, 1, 4918–4926.
- (54) Hentschke, R. On The Specific Heat Capacity Enhancement in Nanofluids. Nanoscale Res. Lett. **2016**, 11, 1–11.

- (55) Shu, J.-J.; Bin Melvin Teo, J.; Kong Chan, W. Fluid Velocity Slip and Temperature Jump At a Solid Surface. Appl. Mech. Rev. 2017, 69.
- (56) Caplan, M. E.; Giri, A.; Hopkins, P. E. Analytical Model For The Effects of Wetting On Thermal Boundary Conductance Across Solid/Classical Liquid Interfaces. J. Chem. Phys. 2014, 140, 154701.
- (57) D'Aguanno, B.; Karthik, M.; Grace, A.; Floris, A. Thermostatic Properties of Nitrate Molten Salts and Their Solar and Eutectic Mixtures. *Sci. Rep.* **2018**, *8*, 1–15.
- (58) Bolmatov, D.; Zhernenkov, M.; Zav'yalov, D.; Cai, Y. Q.; Cunsolo, A. Terasonic Excitations in 2D Gold Nanoparticle Arrays in A Water Matrix as Revealed by Atomistic Simulations. *J. Phys. Chem. C* **2016**, *120*, 19896–19903.
- (59) Giri, A.; Hopkins, P. E. Spectral Analysis of Thermal Boundary Conductance Across Solid/Classical Liquid Interfaces: A Molecular Dynamics Study. Appl. Phys. Lett. 2014, 105, 033106.
- (60) Kim, Y.; Yanaba, Y.; Morita, K. Influence of Structure and Temperature On The Thermal Conductivity of Molten CaO-B2O3. J. Am. Ceram. Soc. 2017, 100, 5746-5754.
- (61) Merabia, S.; Lombard, J.; Alkurdi, A. Importance of Viscoelastic And Interface Bonding Effects in The Thermal Boundary Conductance of Solid-Water Interfaces. Int. J. Heat Mass Transf. 2016, 100, 287–294.
- (62) Zhang, H.; Duquesne, M.; Godin, A.; Niedermaier, S.; del Barrio, E. P.; Nedea, S. V.; Rindt, C. C. Experimental and In Silico Characterization of Xylitol as Seasonal Heat Storage Material. Fluid Ph. Equilibria 2017, 436, 55–68.

- (63) Frank, M.; Drikakis, D. Solid-like Heat Transfer in Confined Liquids. *Microfluid.* Nanofluidics **2017**, 21, 1–6.
- (64) Keanini, R. G.; Dahlberg, J.; Tkacik, P. T. On the Physical Mechanisms Underlying Single Molecule Dynamics in Simple Liquids. Sci. Rep. 2021, 11, 1–18.
- (65) Frank, M.; Drikakis, D. Thermodynamics at Solid-Liquid Interfaces. *Entropy* **2018**, *20*, 362.
- (66) Song, D.-X.; Ma, W.-G.; Zhang, X. Anisotropic Thermal Conductivity in Ferrofluids Induced by Uniform Cluster Orientation and Anisotropic Phonon Mean Free Path. *Int. J. Heat Mass Transf.* **2019**, *138*, 1228–1237.
- (67) Tanase, M.; Soare, A.; David, V.; Moldoveanu, S. C. Sources of Nonlinear van't Hoff Temperature Dependence in High-Performance Liquid Chromatography. ACS Omega 2019, 4, 19808–19817.
- (68) Ghosh, K.; Krishnamurthy, C. Frenkel Line Crossover of Confined Supercritical Fluids. Sci. Rep. **2019**, 9, 1–14.
- (69) Yoon, T. J.; Ha, M. Y.; Lazar, E. A.; Lee, W. B.; Lee, Y.-W. Topological Characterization of Rigid-Nonrigid Transition Across The Frenkel Line. *J. Phys. Chem. Lett.* **2018**, *9*, 6524–6528.
- (70) English, N. J.; Tse, J. S. Thermal Conductivity of Supercooled Water: An Equilibrium Molecular Dynamics Exploration. J. Phys. Chem. Lett. 2014, 5, 3819–3824.
- (71) Tomko, J. A.; Olson, D. H.; Giri, A.; Gaskins, J. T.; Donovan, B. F.; O'Malley, S. M.; Hopkins, P. E. Nanoscale Wetting and Energy Transmission at Solid/Liquid Interfaces. *Langmuir* 2019, 35, 2106–2114.
- (72) Gonzalez-Valle, C. U.; Paniagua-Guerra, L. E.; Ramos-Alvarado, B.

- Implications of the Interface Modeling Approach on the Heat Transfer across Graphite–Water Interfaces. *J. Phys. Chem. C* **2019**, *123*, 22311–22323.
- (73) Yoon, T. J.; Ha, M. Y.; Lee, W. B.; Lee, Y.-W.; Lazar, E. A. Topological Generalization of The Rigid-Nonrigid Transition in Soft-Sphere and Hard-Sphere Fluids. *Phys. Rev. E* **2019**, *99*, 052603.
- (74) Stamper, C.; Cortie, D.; Yue, Z.; Wang, X.; Yu, D. Experimental Confirmation of the Universal Law for the Vibrational Density of States of Liquids. J. Phys. Chem. Lett. 2022, 13, 3105–3111.
- (75) Engelmann, S.; Hentschke, R. Specific Heat Capacity Enhancement Studied in Silica Doped Potassium Nitrate via Molecular Dynamics Simulation. *Sci. Rep.* **2019**, *9*, 1–14.
- (76) Song, D.-X.; Zhang, Y.-F.; Ma, W.-G.; Zhang, X. Role of Electron–Phonon Coupling in Thermal Conductivity of Metallic Nanofluids. *J. Phys. D: Appl. Phys* **2019**, *52*, 485302.
- (77) Lilley, D.; Jain, A.; Prasher, R. A Simple Model for The Entropy of Melting of Monatomic Liquids. *Appl. Phys. Lett.* **2021**, *118*, 083902.
- (78) Proctor, J. E. Modeling of Liquid Internal Energy and Heat Capacity Over a Wide Pressure–Temperature Range from First Principles. *Phys. Fluids* **2020**, *32*, 107105.
- (79) Zhao, A. Z.; Wingert, M. C.; Chen, R.; Garay, J. E. Phonon Gas Model for Thermal Conductivity of Dense, Strongly Interacting Liquids. J. Appl. Phys. 2021, 129, 235101.
- (80) Ayrinhac, S. Heat Capacity Ratio in Liquids at High Pressure. *J. Appl. Phys.* **2021**, *129*, 185903.

- (81) Pruteanu, C. G.; Proctor, J. E.; Alderman, O. L.; Loveday, J. S. Structural Markers of The Frenkel Line in The Proximity of Widom Lines. J. Phys. Chem. B 2021, 125, 8902–8906.
- (82) Ojovan, M. I.; Louzguine-Luzgin, D. V. On Structural Rearrangements during The Vitrification of Molten Copper. *Materials* **2022**, *15*, 1313.
- (83) Leonardi, E.; Floris, A.; Bose, S.; D'Aguanno, B. Unified Description of the Specific Heat of Ionic Bulk Materials Containing Nanoparticles. ACS nano 2020, 15, 563-574.
- (84) Chen, G. Perspectives on Molecular-Level Understanding of Thermophysics of Liquids and Future Research Directions. J Heat Transfer 2022, 144.
- (85) Ghandili, A.; Moeini, V. A General Model for Isochoric Heat Capacity of Matter in Different States by Introducing Thermodynamic Dimension Concept. Fluid Ph. Equilibria 2022, 555, 113355.
- (86) Trachenko, K.; Brazhkin, V.; Bolmatov, D. Dynamic Transition of Supercritical Hydrogen: Defining The Boundary Between Interior and Atmosphere in Gas Giants. *Phys. Rev. E* **2014**, *89*, 032126.
- (87) Bolmatov, D.; Zav'yalov, D.; Gao, M.; Zhernenkov, M. Structural Evolution of Supercritical CO2 Across The Frenkel Line. *J. Phys. Chem. Lett.* **2014**, *5*, 2785–2790.
- (88) Bolmatov, D.; Brazhkin, V.; Trachenko, K. Helium At Elevated Pressures: Quantum Liquid With Non-static Shear Rigidity. J. Appl. Phys. **2013**, 113, 103514.
- (89) Bolmatov, D.; Zhernenkov, M.; Sharpnack, L.; Agra-Kooijman, D. M.; Kumar, S.; Suvorov, A.; Pindak, R.; Cai, Y. Q.; Cunsolo, A. Emergent Optical Phononic Modes upon Nanoscale

- Mesogenic Phase Transitions. *Nano Lett.* **2017**, *17*, 3870–3876.
- (90) Bolmatov, D.; Soloviov, D.; Zav'yalov, D.; Sharpnack, L.; Agra-Kooijman, D. M.; Kumar, S.; Zhang, J.; Liu, M.; Katsaras, J. Anomalous Nanoscale Optoacoustic Phonon Mixing in Nematic Mesogens. J. Phys. Chem. Lett. 2018, 9, 2546–2553.
- (91) Zhernenkov, M.; Bolmatov, D.; Soloviov, D.; Zhernenkov, K.; Toperverg, B. P.; Cunsolo, A.; Bosak, A.; Cai, Y. Q. Revealing the Mechanism of Passive Transport in Lipid Bilayers via Phonon-Mediated Nanometre-Scale Density Fluctuations. *Nat. Commun.* **2016**, 7, 1–10.
- (92) Bolmatov, D.; Soloviov, D.; Zhernenkov, M.; Zav'yalov, D.; Mamontov, E.; Suvorov, A.; Cai, Y. Q.; Katsaras, J. Molecular Picture of the Transient Nature of Lipid Rafts. *Langmuir* **2020**, *36*, 4887–4896.
- (93) Bolmatov, D.; Carrillo, J.-M. Y.; Sumpter, B. G.; Katsaras, J.; Lavrentovich, M. O. Double Membrane Formation in Heterogeneous Vesicles. Soft Matter 2020, 16, 8806–8817.
- (94) Bolmatov, D.; Kinnun, J. J.; Katsaras, J.; Lavrentovich, M. O. Phonon-Mediated Lipid Raft Formation in Biological Membranes. *Chem. Phys. Lipids* **2020**, *232*, 104979.
- (95) D'Angelo, G.; Nibali, V. C.; Wanderlingh, U.; Branca, C.; De Francesco, A.; Sacchetti, F.; Petrillo, C.; Paciaroni, A. Multiple Interacting Collective Modes and Phonon Gap in Phospholipid Membranes. J. Phys. Chem. Lett. 2018, 9, 4367–4372.
- (96) Bolmatov, D.; Cai, Y. Q.; Zav'yalov, D.; Zhernenkov, M. Crossover from Picosecond Collective to Single Particle Dynamics Defines the Mechanism of Lateral

- Lipid Diffusion. Biochimica et Biophysica Acta (BBA)-Biomembranes **2018**, 1860, 2446–2455.
- (97) Bolmatov, D.; Zav'yalov, D.; Carrillo, J.-M.; Katsaras, J. Fractal Boundaries Underpin the 2D Melting of Biomimetic Rafts. *Biochimica et Biophysica Acta* (BBA)-Biomembranes **2020**, 1862, 183249.
- (98) Reiter, R. J. Pineal Melatonin: Cell Biology of Its Synthesis and of Its Physiological Interactions. *Endocr. Rev.* **1991**, 12, 151–180.
- (99) Bolmatov, D.; Lavrentovich, M. O.; Reiter, R. J. Molecular Interactions of Melatonin with Lipid Rafts. *Melatonin Res.* **2022**, *5*, 101–113.
- (100) Bolmatov, D.; McClintic, W. T.; Taylor, G.; Stanley, C. B.; Do, C.; Collier, C. P.; Leonenko, Z.; Lavrentovich, M. O.; Katsaras, J. Deciphering Melatonin-Stabilized Phase Separation in Phospholipid Bilayers. *Langmuir* **2019**, *35*, 12236–12245.
- (101) Nibali, V. C.; D'Angelo, G.; Tarek, M. Molecular Dynamics Simulation of Short-Wavelength Collective Dynamics of Phospholipid Membranes. *Phys. Rev.* E 2014, 89, 050301.
- (102) Vaz, W. L.; Clegg, R. M.; Hallmann, D. Translational diffusion of lipids in liquid crystalline phase phosphatidylcholine multibilayers. A comparison of experiment with theory. *Biochemistry* **1985**, 24, 781–786.
- (103) Lindblom, G.; Orädd, G.; Filippov, A. Lipid lateral diffusion in bilayers with phosphatidylcholine, sphingomyelin and cholesterol: An NMR study of dynamics and lateral phase separation. *Chem. Phys. Lipids* **2006**, *141*, 179–184.
- (104) Scheidt, H. A.; Huster, D.; Gawrisch, K. Diffusion of cholesterol and its precursors in lipid membranes studied by 1H

- pulsed field gradient magic angle spinning NMR. *Biophys. J.* **2005**, *89*, 2504–2512.
- (105) Almeida, P. F.; Vaz, W. L.; Thompson, T. Lateral diffusion in the liquid phases of dimyristoylphosphatidylcholine/cholesterol lipid bilayers: a free volume analysis. *Biochemistry* **1992**, *31*, 6739–6747.
- (106) Mendil, H.; Baroni, P.; Noirez, L. Solid-Like Rheological Response of Non-Entangled Polymers in the Molten State. *Eur. Phys. J. E* **2006**, *19*, 77–85.
- (107) Noirez, L.; Baroni, P. Identification of Thermal Shear Bands in a Low Molecular Weight Polymer Melt under Oscillatory Strain Field. *Colloid Polym. Sci.* **2018**, 296, 713–720.
- (108) Kume, E.; Baroni, P.; Noirez, L. Strain-Induced Violation of Temperature Uniformity in Mesoscale Liquids. *Sci. Rep.* **2020**, *10*, 1–7.
- (109) Zaccone, A.; Trachenko, K. Explaining the Low-Frequency Shear Elasticity of Confined Liquids. *Proc. Natl. Acad. Sci. U.S.A.* **2020**, *117*, 19653–19655.
- (110) Maldovan, M. Sound and Heat Revolutions in Phononics. *Nature* **2013**, *503*, 209–217.
- (111) Zaccone, A.; Baggioli, M. Universal Law for the Vibrational Density of States of Liquids. *Proc. Natl. Acad. Sci. U.S.A.* **2021**, *118*.
- (112) Anishkin, A.; Loukin, S. H.; Teng, J.; Kung, C. Feeling the Hidden Mechanical Forces in Lipid Bilayer is an Original Sense. *Proc. Natl. Acad. Sci. U.S.A.* 2014, 111, 7898–7905.
- (113) Teng, J.; Loukin, S.; Anishkin, A.; Kung, C. The Force-From-Lipid (FFL) Principle of Mechanosensitivity, at Large and in Elements. Eur. J. Appl. Physiol. **2015**, 467, 27–37.

- (114) Wallis, T. P.; Venkatesh, B. G.; Narayana, V. K.; Kvaskoff, D.; Ho, A.; Sullivan, R. K.; Windels, F.; Sah, P.; Meunier, F. A. Saturated Free Fatty Acids and Association with Memory Formation. *Nat. Commun.* **2021**, *12*, 1–11.
- (115) Martin, S. J.; Grimwood, P. D.; Morris, R. G. Synaptic Plasticity and Memory: an Evaluation of the Hypothesis. *Annu. Rev. Neurosci.* **2000**, *23*, 649–711.
- (116) Neves, G.; Cooke, S. F.; Bliss, T. V. Synaptic Plasticity, Memory and the Hippocampus: a Neural Network Approach to Causality. *Nat. Rev. Neurosci.* **2008**, *9*, 65–75.
- (117) Najem, J. S.; Hasan, M. S.; Williams, R. S.; Weiss, R. J.; Rose, G. S.; Taylor, G. J.; Sarles, S. A.; Collier, C. P. Dynamical Nonlinear Memory Capacitance in Biomimetic Membranes. *Nat. Commun.* **2019**, *10*, 1–11.
- (118) Sacci, R. L.; Scott, H. L.; Liu, Z.; Bolmatov, D.; Doughty, B.; Katsaras, J.; Collier, C. P. Disentangling Memristive and Memcapacitive Effects in Droplet Interface Bilayers Using Dynamic Impedance Spectroscopy. Adv. Electron. Mater. 2022, 8, 2200121.
- (119) Abraham, W. C.; Jones, O. D.; Glanzman, D. L. Is Plasticity of Synapses the Mechanism of Long-Term Memory Storage? NPJ Sci. Learn. 2019, 4, 1–10.
- (120) Levental, I.; Veatch, S. L. The Continuing Mystery of Lipid Rafts. *J. Mol. Biol.* **2016**, *428*, 4749–4764.
- (121) Soloviov, D.; Cai, Y. Q.; Bolmatov, D.; Suvorov, A.; Zhernenkov, K.; Zav'yalov, D.; Bosak, A.; Uchiyama, H.; Zhernenkov, M. Functional Lipid Pairs as Building Blocks of Phase-Separated Membranes. *Proc. Natl. Acad. Sci. U.S.A.* **2020**, *117*, 4749–4757.
- (122) Benucci, A.; Frazor, R. A.; Carandini, M. Standing Waves and Traveling Waves

- Distinguish Two Circuits in Visual Cortex. *Neuron* **2007**, *55*, 103–117.
- (123) Bhattacharya, S.; Brincat, S. L.; Lundqvist, M.; Miller, E. K. Traveling Waves in the Prefrontal Cortex during Working Memory. *PLoS Comput. Biol.* **2022**, *18*, e1009827.
- (124) Bhattacharya, S.; Banerjee, T.; Miao, Y.; Zhan, H.; Devreotes, P. N.; Iglesias, P. A. Traveling and Standing Waves Mediate Pattern Formation in Cellular Protrusions. Sci. Adv. 2020, 6, eaay7682.